Rapid Communications

Spin-excitation anisotropy in the bilayer iron-based superconductor $CaKFe_4As_4$

Tao Xie,[1,2] Chang Liu,[1,2] Frédéric Bourdarot,[3] Louis-Pierre Regnault,[4] Shiliang Li,[1,2,5] and Huiqian Luo[1,5,*]

[1]*Beijing National Laboratory for Condensed Matter Physics, Institute of Physics, Chinese Academy of Sciences, Beijing 100190, China*

[2]*University of Chinese Academy of Sciences, Beijing 100049, China*

[3]*Université Grenoble Alpes, CEA, INAC, MEM MDN, F-38000 Grenoble, France*

[4]*Institut Laue-Langevin, 71 avenue des Martyrs, CS 20156, 38042 Grenoble Cedex, France*

[5]*Songshan Lake Materials Laboratory, Dongguan, Guangdong 523808, China*

(Received 2 March 2020; accepted 2 April 2020; published 27 April 2020)

We use polarized inelastic neutron scattering to study the spin-excitation anisotropy in the bilayer iron-based superconductor $CaKFe_4As_4$ ($T_c = 35$ K). In the superconducting state, both odd and even L modulations of spin resonance have been observed in our previous unpolarized neutron-scattering experiments [Xie *et al.*, Phys. Rev. Lett. **120**, 267003 (2018)]. Here we find that the high-energy even mode (∼18 meV) is isotropic in spin space, but the low-energy odd modes consist of a c-axis polarized mode around 9 meV along with another partially overlapped in-plane mode around 12 meV. We argue that such spin anisotropy is induced by the spin-orbit coupling in the spin-vortex-type fluctuations of this unique compound. The spin anisotropy is strongly affected by the superconductivity, where it is weak below 6 meV in the normal state and then transferred to higher energy and further enhanced in the odd modes of spin resonance below T_c.

DOI: 10.1103/PhysRevResearch.2.022018

The neutron spin resonance, a collective mode of spin excitations that appears at a specific energy around the antiferromagnetic (AF) wave vector of the parent compounds in the superconducting state, is generally believed to be a crucial evidence for the spin-fluctuations-mediated superconducting pairing in unconventional superconductors [1–7]. Theoretically, the spin resonance mode is argued to be a collective bosonic mode from singlet-triplet excitations of the Cooper pairs, and thus it is expected to be isotropic in the spin space due to its spin-1 nature [5]. However, the case in iron-based superconductors is much more complicated. Considering the fact that the spin excitations in these materials have both local-moment and itinerant characteristics [1–3], either by approximating to the parent compound with strong single-ion anisotropy [8–10] or being affected by the orbital ordering via spin-orbit coupling (SOC) [11–13], a spin anisotropy can be present in the spin resonance mode. While the spin anisotropy commonly exists in the low-energy spin excitations and even persists into high temperature well above the Néel temperature T_N, the anisotropy of the spin resonance is different among the iron-based superconductors [14–26]. For example, the spin resonance mode in the 11-type compound FeSe seems to be purely c-axis polarized [25], but in the 112-type compound $Ca_{1-y}La_yFe_{1-x}Ni_xAs_2$, it is completely isotropic [26]. In the 122-type systems such as K-, Co-, Ni-, or P-doped $BaFe_2As_2$ compounds, although the spin resonance modes are either c-axis polarized or weakly a-axis polarized [14–17,20–22], the maximum energies of spin anisotropy in the superconducting state have been found to be linearly scaling with their superconducting critical temperature T_c [21,22].

To further understand the spin anisotropy of the spin resonance and the role of the SOC in iron-based superconductivity, we have performed polarized neutron-scattering experiments on a stoichiometric iron-based superconductor $CaKFe_4As_4$ with $T_c = 35$ K [Fig. 1(a)] [27,28]. In this compound, neither the tetragonal-orthorhombic structural transition related to the nematic order nor the long-ranged magnetic order with single-ion anisotropy exists, and the absence of chemical dopants gives a minimum disorder effect from local impurity. However, the SOC may also exist in $CaKFe_4As_4$, since it may naturally close to a quantum critical point of a hedgehog spin-vortex crystal (SVC) order, which is discovered in those Ni- or Co-doped compounds and has two perpendicularly ordered moments with equal magnitudes within the ab plane [29,30]. Previously, our unpolarized neutron-scattering experiments have revealed triple resonance modes around 9.5, 13, and 18.3 meV [Figs. 1(d) and 1(e)] [31]. All of them show strong L modulations, which can be classified into odd and even symmetries with respect to the Fe-Fe distance within one Fe-As bilayer unit [Figs. 1(c)–1(e)] [31–34]. Such separated multiple resonance modes from nondegenerate spin excitations offer a unique chance to study the spin anisotropy of each mode. Here, by using polarized neutron-scattering analysis [Fig. 1(b)], we have found that the high-energy even mode of spin resonance is isotropic, while the low-energy odd modes become pronouncedly anisotropic with a c-axis polarized mode around 9 meV overlapped with a weakly anisotropic in-plane mode around 12 meV. The maximum energy of spin anisotropy also follows the linear scaling with T_c, as shown in doped $BaFe_2As_2$ systems [Fig. 1(f)]. The spin

*hqluo@iphy.ac.cn

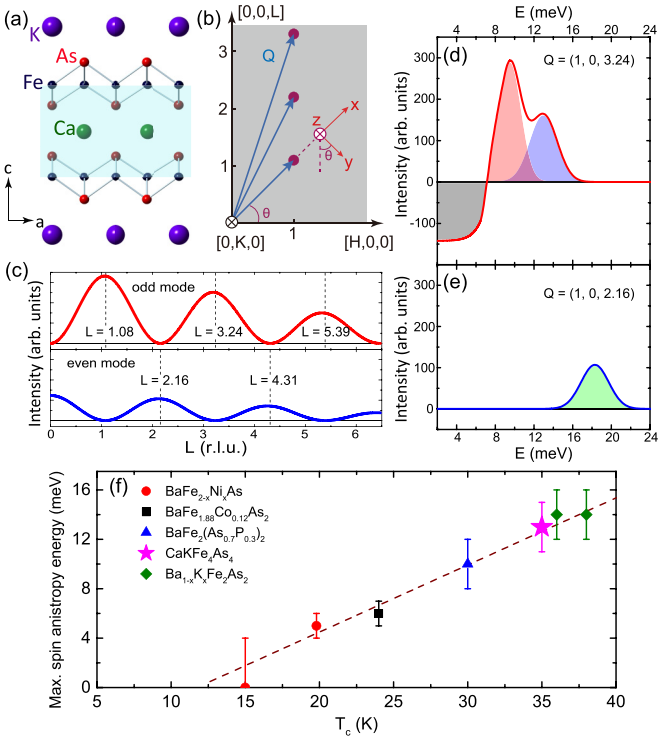

FIG. 1. (a) Crystal structure of $CaKFe_4As_4$. The lattice axes are indicated in the tetragonal notation; the blue shadow area indicates the Fe-As bilayer unit. (b) The scattering plane and the definition of the spin-polarization directions in the reciprocal space. (c) Odd and even L symmetries of the spin resonance. The dashed lines indicate the nonintegral L positions with maximum intensities. (d),(e) Schematic diagrams of three spin resonance modes at $\mathbf{Q} = (1, 0, 3.24)$ (odd modes) and $\mathbf{Q} = (1, 0, 2.16)$ (even mode) deduced from the intensity differences between $T = 1.5$ and 40 K [31]. (f) Linear scaling between the maximum spin-anisotropy energy and T_c.

anisotropy in $CaKFe_4As_4$ can be attributed to the SOC under SVC-type fluctuations. It is pushed to higher energy and then strongly enhanced in the spin resonance after cooling down below T_c.

We used the same set of $CaKFe_4As_4$ single crystals in our previous unpolarized neutron-scattering experiments [31]. The polarized neutron-scattering experiments were carried out using the CryoPAD system at the CEA-CRG IN22 thermal triple-axis spectrometer in Institut Laue-Langevin, Grenoble, France, with a fixed final energy $E_f = 14.7$ meV. The CryoPAD system provides a strictly zero magnetic field environment for the measured sample, thus avoiding errors due to flux inclusion and field expulsion in the superconducting state of the sample [35]. The scattering plane $[H, 0, 0] \times [0, 0, L]$ is defined using the same magnetic unit cell as before [31]: $a_M = b_M = 5.45$ Å, $c = 12.63$ Å, in which the wave vector $\mathbf{Q}$ at (q_x, q_y, q_z) is $(H, K, L) = (q_x a_M/2\pi, q_y b_M/2\pi, q_z c/2\pi)$ reciprocal lattice units (r.l.u.). We defined the neutron-polarization directions as x, y, z, with x parallel to $\mathbf{Q}$, and y (in scattering plane) and z (out of scattering plane) perpendicular to $\mathbf{Q}$, as shown in Fig. 1(b). Since the spin of a neutron has a tendency to flip (spin flip: SF) after a scattering event with the magnetic excitations from the sample, the three neutron SF scattering cross sections can be written as σ_x^{SF}, σ_y^{SF}, and σ_z^{SF}. Because neutron SF scattering is only sensitive to the magnetic excitations/moments that are perpendicular to the momentum transfer $\mathbf{Q}$ and the neutron spin-polarization directions [14,15,24], in our geometry,

$$\begin{aligned} \sigma_x^{\mathrm{SF}} &= cM_y + cM_z + B, \\ \sigma_y^{\mathrm{SF}} &= cM_z + B, \\ \sigma_z^{\mathrm{SF}} &= cM_y + B. \end{aligned} \tag{1}$$

Here, M_y and M_z are the magnitudes of magnetic excitations along the y and z directions, B is the constant background, and $c = (R - 1)/(R + 1)$. The spin-flipping ratio R represents the quality of the neutron spin polarization, defined by the leakage of nuclear Bragg peaks (should be non-spin-flip: NSF) into the SF channel: $R = \sigma_{\mathrm{nuclear}}^{\mathrm{NSF}}/\sigma_{\mathrm{nuclear}}^{\mathrm{SF}}$, which is about 13 in our experiments. From Eq. (1), the background can be estimated by comparing the SF scattering between all three channels, which is $B = \sigma_y^{\mathrm{SF}} + \sigma_z^{\mathrm{SF}} - \sigma_x^{\mathrm{SF}}$. M_y and M_z in Eq. (1) can be further written as the combinations of the magnetic excitations along the lattice axes a_M, b_M, and c:

$$\begin{aligned} M_y &= M_a \sin^2\theta + M_c \cos^2\theta, \\ M_z &= M_b, \end{aligned} \tag{2}$$

where θ is the angle between $\mathbf{Q}$ and the $(H, 0, 0)$ direction [Fig. 1(b)]. By measuring the SF scattering cross sections at least two unparallel $\mathbf{Q}$ positions with same energy transfer, we can deduce all three components M_a, M_b, and M_c (see Supplemental Material [36]). In this method, we do not have to assume $M_a = M_b$ in the calculation [9,17,21,22,26], even though it is very likely in this stoichiometric material with a tetragonal lattice structure [27,28].

Since the maximum intensities of the spin resonance modes locate at noninteger L positions such as $L = 1.08$, 3.24, and 5.39 for the odd modes, and $L = 2.16$, 4.31, and 6.47 for the even mode [Fig. 1(c)] [31], we picked the noninteger L indexes $L = 1.1$, 2.2, and 3.3 to do the measurements for accuracy. Figure 2 gives the raw-energy scans of σ_x^{SF}, σ_y^{SF}, and σ_z^{SF} at $\mathbf{Q} = (1, 0, L)$. In contrast to the almost featureless results in the normal state [Figs. 2(b), 2(d), and 2(f)], the spin excitations in the superconducting state show clear spin resonance peaks [Figs. 2(a), 2(c), and 2(e)] around 18 meV for $L = 2.2$ (even mode) and 10 meV for $L = 1.1$ and $L = 3.3$ (odd modes) in all the SF channels. These observed spin resonance modes are consistent with the previous unpolarized results [31]. If the spin excitations are isotropic in spin space, there will be no difference between M_y and M_z, and thus $\sigma_y^{\mathrm{SF}} = \sigma_z^{\mathrm{SF}} = (\sigma_x^{\mathrm{SF}} + B)/2$ [17,26]. It is indeed the case at $\mathbf{Q} = (1, 0, 2.2)$ in both the superconducting and normal states [Figs. 2(a) and 2(b)], suggesting that the even mode is completely isotropic, while the results for the odd modes at $\mathbf{Q} = (1, 0, 3.3)$ and $(1, 0, 1.1)$ are very different. In detail, in the superconducting state, the spin excitations are remarkably anisotropic in the energy window $E \sim 6-15$ meV for the odd modes of spin resonance, and there is a full spin gap below 5 meV due to the identical intensities for all three channels ($\sigma_x^{\mathrm{SF}} = \sigma_y^{\mathrm{SF}} = \sigma_z^{\mathrm{SF}}$), which only measures the isotropic backgrounds [Figs. 2(c) and 2(e)]. Above T_c, the signals become almost isotropic except for a weak anisotropy remaining at low energies below 6 meV [Figs. 2(d) and 2(f)]. The intensity

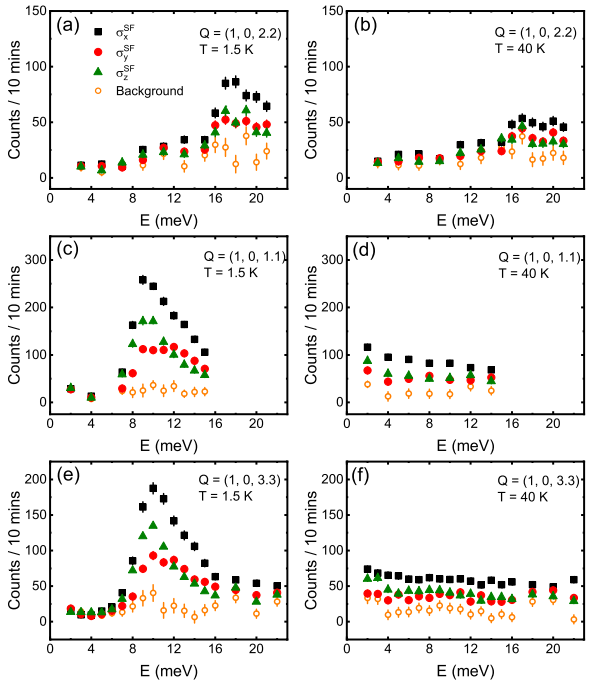

FIG. 2. Raw data of constant-**Q** scans of $\sigma_x^{\rm SF}$, $\sigma_y^{\rm SF}$, and $\sigma_z^{\rm SF}$ at $\mathbf{Q} = (1, 0, L)$ with (a) $L = 2.2$, (c) $L = 1.1$, and (e) $L = 3.3$ at 1.5 K (superconducting state) and (b) $L = 2.2$, (d) $L = 1.1$, and (f) $L = 3.3$ at 40 K (normal state). Open circles are the background estimated using $B = \sigma_y^{\rm SF} + \sigma_z^{\rm SF} - \sigma_x^{\rm SF}$.

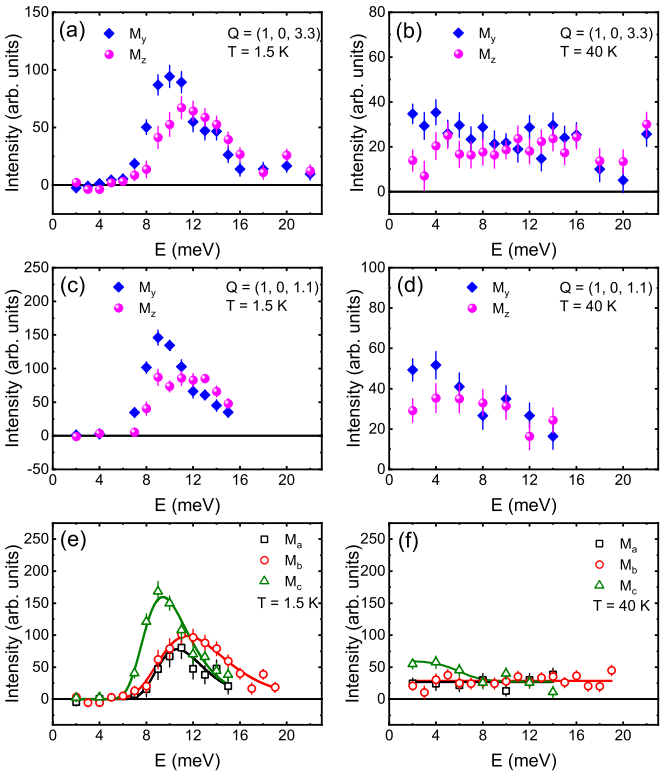

FIG. 3. (a), (b) Energy dependence of M_y and M_z at $\mathbf{Q} = (1, 0, 3.3)$ below and above T_c. (c), (d) Energy dependence of M_y and M_z at $\mathbf{Q} = (1, 0, 1.1)$ below and above T_c. (e), (f) Energy dependence of M_a, M_b, and M_c below and above T_c, where the solid lines are guides to the eyes.

differences between $\mathbf{Q} = (1, 0, 3.3)$ and $(1, 0, 1.1)$ come from the magnetic form factor and the instrument resolution effects (see Ref. [17] and Supplemental Material [36]).

Using Eq. (1), we can obtain the magnitudes of magnetic excitations along the y- and z-polarization directions: $cM_y = \sigma_x^{\rm SF} - \sigma_y^{\rm SF}$ and $cM_z = \sigma_x^{\rm SF} - \sigma_z^{\rm SF}$. The intensity difference of spin excitations along the y and z directions displays the anisotropic behavior more visually [Figs. 3(a)–3(d)]. With M_y and M_z derived from two equivalent **Q** positions, $\mathbf{Q} = (1, 0, 1.1)$ and $\mathbf{Q} = (1, 0, 3.3)$, we can further calculate M_a, M_b, and M_c from Eq. (2). The angle θ between **Q** and $\mathbf{a}^*$ for $L = 1.1$ and 3.3 is 25.5° and 55°, respectively (see Supplemental Material [36]). Figures 3(e) and 3(f) display the energy dependence of M_a, M_b, and M_c in the superconducting state and normal state, respectively. We can identify a c-axis polarized resonance mode around 9 meV overlapped with another weakly anisotropic in-plane mode around 12 meV, corresponding to the two overlapped odd modes in the previous unpolarized report [31]. The spin gap of all channels seems to develop at the same energy, $E = 6$ meV. The weak anisotropy in the normal state at low energy is also partially c-axis polarized below 6 meV, as shown in Fig. 3(f).

To track the anisotropy of spin gap and spin resonance induced by the superconducting transition in $CaKFe_4As_4$, we have performed temperature scans at $\mathbf{Q} = (1, 0, 3.3)$ with energy transfer $E = 2$ and 10 meV, and the results are shown in Fig. 4. At $E = 2$ meV, the spin anisotropy of $\sigma_z^{\rm SF} > \sigma_y^{\rm SF}$ ($M_y > M_z$) can be clearly seen in the normal state and gradually becomes invisible below T_c for the zero intensity of the full spin gap opening in all the SF channels [Figs. 4(a) and 4(c)]. For $E = 10$ meV, the results are completely opposite: the same type of spin anisotropy ($M_y > M_z$) develops only below T_c when entering into the superconducting state [Figs. 4(b) and 4(d)]. Such intimate relationships between the spin anisotropy and the superconducting transition indicate that the spin anisotropy is strongly affected by the superconductivity in $CaKFe_4As_4$.

The spin anisotropy in $CaKFe_4As_4$ gives us clues to understand the SOC in the superconducting state. First, the spin anisotropy solely presented in the odd modes of spin resonance most likely originates from the SOC. Since the odd and even modes of spin resonance are corresponding to the symmetric and antisymmetric states of the nondegenerate magnetic excitations in the FeAs interbilayer [31–34], both of them should be isotropic in spin space, assuming that the spin resonance is indeed from a spin-1 exciton of the singlet Cooper pairs and there is no SOC. However, with sufficient SOC, the orbital-selective electron correlations and superconducting pairings would possibly introduce spin-excitation anisotropy [11–13]. Second, the spin anisotropy from SOC is limited at low-energy spin excitations, both in the normal state and the superconducting state, and thus the high-energy even mode of spin resonance can remain isotropic. In fact, for many iron-based superconductors explored so far, the anisotropy of spin resonance mostly exists at the low-energy part of the resonance peak, while above E_R, it is nearly isotropic [16–25]. In the FeSe system with sufficiently low T_c (about 8 K) and

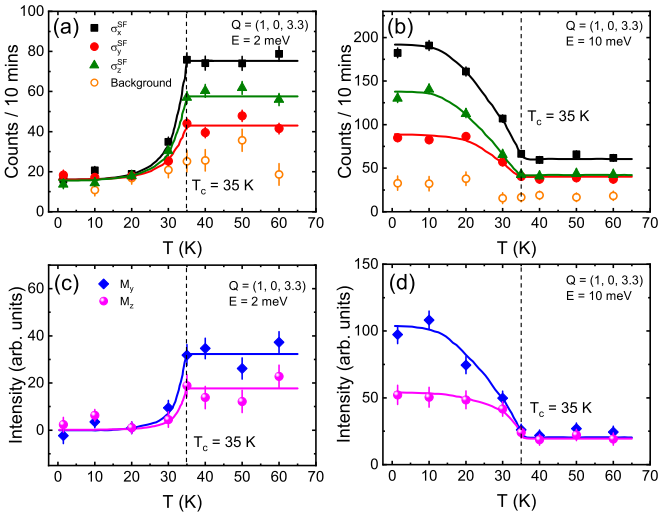

FIG. 4. (a), (b) Temperature dependence of the σ_x^{SF}, σ_y^{SF}, and σ_z^{SF} at $\mathbf{Q} = (1, 0, 3.3)$ at 2 and 10 meV, where the open circles are estimated backgrounds. (c), (d) Temperature dependence of the M_y and M_z at $\mathbf{Q} = (1, 0, 3.3)$ at 2 and 10 meV. The solid lines are guides to the eyes. The vertical dashed lines indicate T_c.

E_R (about 4 meV), the spin resonance peak can be fully c-axis polarized [25]. Third, the SOC is significantly enhanced in the superconducting state. The superconducting gap opening below T_c not only evokes the collective spin resonance modes, but also partially even fully gaps the low-energy spin excitations. This effect transfers the small spin anisotropy in the normal state to higher energy, which is boosted by the spin resonance in the superconducting state. Because the resonance energy is proportional to the superconducting gaps and T_c [26,31], a positive relation between the maximum energy of spin anisotropy and T_c would be expected in those iron-based superconductors with similar strength of SOC [Fig. 1(f)] [21,22].

The character of SOC is an important key to understand the magnetic structure and superconductivity in the iron-based superconductors [25,37,38]. In fact, the SOC-induced axis-polarized intensity of the spin resonance mode is usually attributed to a proximity to a possible AF instability or structural transition [16–25]. Although the stoichiometric $CaKFe_4As_4$ is naturally paramagnetic, a C_4 symmetric SVC phase with ordered moments within the ab plane emerges after doping 3.3% Ni or 7.2% Co to suppress the superconductivity below 20 K, where two wave vectors have equal magnitudes in an orthogonal geometry ($\langle|\mathbf{M_1}|\rangle = \langle|\mathbf{M_2}|\rangle \neq 0$, $\langle\mathbf{M_1}\rangle \cdot \langle\mathbf{M_2}\rangle = 0$) [29,30]. Unlike the Ising-nematic order in the stripe-type AF structure, the SVC phase has an order parameter ($\varphi = \langle\mathbf{M_1} \times \mathbf{M_2}\rangle$) that breaks the spin-rotational symmetry from $O(3)$ to $O(2)$ and produces chiral spin currents together with strong SOC [39]. In other words, assuming one of the moments $\mathbf{M_1}$ is fixed, another moment $\mathbf{M_2}$ would prefer to fluctuate in the plane perpendicular to the easy plane (ab plane), giving c-axis polarized magnetic excitations (M_c) at low energy first. The other two modes within the easy plane (M_a and M_b) should cost more energy since it requires both $\mathbf{M_1}$ and $\mathbf{M_2}$ to fluctuate simultaneously along their direction or to rotate synchronously within the plane, not to mention the stronger exchange coupling $J_{ab} > J_c$ [2,3,7]. Indeed, this is exactly the case in the spin resonance of $CaKFe_4As_4$ for the asymmetric intensity between the c-axis polarized mode around 9 meV and the in-plane mode around 12 meV, where a slight difference between M_a and M_b is also reasonable due to their different origins. Further polarized neutron-scattering experiments on the Ni/Co-doped $CaKFe_4As_4$ in the spin-vortex state will be helpful to clarify this issue.

In summary, our polarized neutron-scattering analysis of $CaKFe_4As_4$ suggests that the spin anisotropy only emerges in the low-energy odd modes of spin resonance, while the high-energy even mode is demonstrated to be isotropic in spin space. Although the spin anisotropy is weak at the normal state, it can be significantly enhanced by the superconductivity below T_c. The c-axis polarized mode around 9 meV along with the overlapped in-plane mode around 12 meV are probably induced by the SOC in the SVC-type fluctuations.

The raw data are available in Ref. [40].

This work is supported by the National Key Research and Development Program of China (Grants No. 2018YFA0704201, No. 2017YFA0303103, No. 2017YFA0302903, and No. 2016YFA0300502), the National Natural Science Foundation of China (Grants No. 11822411, No. 11961160699, No. 11674406, and No. 11674372), and the Strategic Priority Research Program (B) of the Chinese Academy of Sciences (CAS) (Grants No. XDB25000000 and No. XDB07020300). H.L. is grateful for the support from the Youth Innovation Promotion Association of CAS (Grant No. 2016004) and the Beijing Natural Science Foundation (Grant No. JQ19002). This work is based on the experiment (4-02-532) performed at the IN22 thermal triple-axis neutron-scattering spectrometer in the Institut Laue-Langevin (ILL), Grenoble, France.

[1] X. Chen, P. Dai, D. Feng, T. Xiang, and F. Zhang, Nation. Sci. Rev. **1**, 371 (2014).
[2] P. Dai, Rev. Mod. Phys. **87**, 855 (2015).
[3] D. S. Inosov, C. R. Phys. **17**, 60 (2016).
[4] J. M. Tranquada, G. Xu, and I. A. Zaliznyak, J. Magn. Magn. Mater. **350**, 148 (2014).
[5] M. Eschrig, Adv. Phys. **55**, 47 (2006).
[6] G. Yu, Y. Li, E. M. Motoyama, and M. Greven, Nat. Phys. **5**, 873 (2009).
[7] P. D. Johnson, G. Xu, and W.-G. Yin, in *Iron-Based Superconductivity* (Springer, New York, 2015), pp. 165–169.
[8] M. Braden, P. Steffens, Y. Sidis, J. Kulda, P. Bourges, S. Hayden, N. Kikugawa, and Y. Maeno, Phys. Rev. Lett. **92**, 097402 (2004).

[9] C. Wang, R. Zhang, F. Wang, H. Luo, L.-P. Regnault, P. Dai, and Y. Li, Phys. Rev. X **3**, 041036 (2013).

[10] Y. Song, X. Lu, L.-P. Regnault, Y. Su, H.-H. Lai, W.-J. Hu, Q. Si, and P. Dai, Phys. Rev. B **97**, 024519 (2018).

[11] P. D. Johnson, H.-B. Yang, J. D. Rameau, G. D. Gu, Z.-H. Pan, T. Valla, M. Weinert, and A. V. Fedorov, Phys. Rev. Lett. **114**, 167001 (2015).

[12] S. V. Borisenko, D. V. Evtushinsky, Z.-H. Liu, I. Morozov, R. Kappenberger, S. Wurmehl, B. Büchner, A. N. Yaresko, T. K. Kim, M. Hoesch, T. Wolf, and N. D. Zhigadlo, Nat. Phys. **12**, 311 (2016).

[13] M. Yi, Y. Zhang, Z.-X. Shen, and D. Lu, npj Quantum Mater. **2**, 57 (2017).

[14] O. J. Lipscombe, L. W. Harriger, P. G. Freeman, M. Enderle, C. Zhang, M. Wang, T. Egami, J. Hu, T. Xiang, M. R. Norman, and P. Dai, Phys. Rev. B **82**, 064515 (2010).

[15] M. Liu, C. Lester, J. Kulda, X. Lu, H. Luo, M. Wang, S. M. Hayden, and P. Dai, Phys. Rev. B **85**, 214516 (2012).

[16] P. Steffens, C. H. Lee, N. Qureshi, K. Kihou, A. Iyo, H. Eisaki, and M. Braden, Phys. Rev. Lett. **110**, 137001 (2013).

[17] H. Luo, M. Wang, C. Zhang, X. Lu, L.-P. Regnault, R. Zhang, S. Li, J. Hu, and P. Dai, Phys. Rev. Lett. **111**, 107006 (2013).

[18] N. Qureshi, C. H. Lee, K. Kihou, K. Schmalzl, P. Steffens, and M. Braden, Phys. Rev. B **90**, 100502(R) (2014).

[19] N. Qureshi, P. Steffens, D. Lamago, Y. Sidis, O. Sobolev, R. A. Ewings, L. Harnagea, S. Wurmehl, B. Büchner, and M. Braden, Phys. Rev. B **90**, 144503 (2014).

[20] C. Zhang, Y. Song, L.-P. Regnault, Y. Su, M. Enderle, J. Kulda, G. Tan, Z. C. Sims, T. Egami, Q. Si, and P. Dai, Phys. Rev. B **90**, 140502(R) (2014).

[21] Y. Song, H. Man, R. Zhang, X. Lu, C. Zhang, M. Wang, G. Tan, L.-P. Regnault, Y. Su, J. Kang, R. M. Fernandes, and P. Dai, Phys. Rev. B **94**, 214516 (2016).

[22] D. Hu, W. Zhang, Y. Wei, B. Roessli, M. Skoulatos, L.-P. Regnault, G. Chen, Y. Song, H. Luo, S. Li, and P. Dai, Phys. Rev. B **96**, 180503(R) (2017).

[23] C. Zhang, M. Liu, Y. Su, L.-P. Regnault, M. Wang, G. Tan, T. Brückel, T. Egami, and P. Dai, Phys. Rev. B **87**, 081101(R) (2013).

[24] P. Babkevich, B. Roessli, S. N. Gvasaliya, L.-P. Regnault, P. G. Freeman, E. Pomjakushina, K. Conder, and A. T. Boothroyd, Phys. Rev. B **83**, 180506(R) (2011).

[25] M. Ma, P. Bourges, Y. Sidis, Y. Xu, S. Li, B. Hu, J. Li, F. Wang, and Y. Li, Phys. Rev. X **7**, 021025 (2017).

[26] T. Xie, D. Gong, H. Ghosh, A. Ghosh, M. Soda, T. Masuda, S. Itoh, F. Bourdarot, L.-P. Regnault, S. Danilkin, S. Li, and H. Luo, Phys. Rev. Lett. **120**, 137001 (2018).

[27] A. Iyo, K. Kawashima, T. Kinjo, T. Nishio, S. Ishida, H. Fujihisa, Y. Gotoh, K. Kihou, H. Eisaki, and Y. Yoshida, J. Am. Chem. Soc. **138**, 3410 (2016).

[28] W. R. Meier, T. Kong, U. S. Kaluarachchi, V. Taufour, N. H. Jo, G. Drachuck, A. E. Böhmer, S. M. Saunders, A. Sapkota, A. Kreyssig, M. A. Tanatar, R. Prozorov, A. I. Goldman, F. F. Balakirev, A. Gurevich, S. L. Bud'ko, and P. C. Canfield, Phys. Rev. B **94**, 064501 (2016).

[29] W. R. Meier, Q.-P. Ding, A. Kreyssig, S. L. Bud′ko, A. Sapkota, K. Kothapalli, V. Borisov, R. Valentí, C. D. Batista, P. P. Orth, R. M. Fernandes, A. I. Goldman, Y. Furukawa, A. E. Böhmer, and P. C. Canfield, npj Quantum Mater. **3**, 5 (2018).

[30] A. Kreyssig, J. M. Wilde, A. E. Böhmer, W. Tian, W. R. Meier, B. Li, B. G. Ueland, M. Xu, S. L. Bud′ko, P. C. Canfield, R. J. McQueeney, and A. I. Goldman, Phys. Rev. B **97**, 224521 (2018).

[31] T. Xie, Y. Wei, D. Gong, T. Fennell, U. Stuhr, R. Kajimoto, K. Ikeuchi, S. Li, J. Hu, and H. Luo, Phys. Rev. Lett. **120**, 267003 (2018).

[32] S. Pailhès, Y. Sidis, P. Bourges, V. Hinkov, A. Ivanov, C. Ulrich, L.-P. Regnault, and B. Keimer, Phys. Rev. Lett. **93**, 167001 (2004).

[33] H. F. Fong, P. Bourges, Y. Sidis, L. P. Regnault, J. Bossy, A. Ivanov, D. L. Milius, I. A. Aksay, and B. Keimer, Phys. Rev. B **61**, 14773 (2000).

[34] Y. Sidis, S. Pailhès, V. Hinkov, B. Fauqué, C. Ulrich, L. Capogna, A. Ivanov, L.-P. Regnault, B. Keimer, and P. Bourges, C. R. Phys. **8**, 745 (2007).

[35] E. Lelièvre-Berna, E. Bourgeat-Lami, P. Fouilloux, B. Geffray, Y. Gibert, K. Kakurai, N. Kernavanois, B. Longuet, F. Mantegezza, M. Nakamura, S. Pujol, L.-P. Regnault, F. Tasset, M. Takeda, M. Thomas, and X. Tonon, Physica B **356**, 131 (2005).

[36] See Supplemental Material at http://link.aps.org/supplemental/10.1103/PhysRevResearch.2.022018 for the details of spin polarization analysis.

[37] M. H. Christensen, J. Kang, and R. M. Fernandes, Phys. Rev. B **100**, 014512 (2019).

[38] J. Guo, L. Yue, K. Iida, K. Kamazawa, L. Chen, T. Han, Y. Zhang, and Y. Li, Phys. Rev. Lett. **122**, 017001 (2019).

[39] R. M. Fernandes, S. A. Kivelson, and E. Berg, Phys. Rev. B **93**, 014511 (2016).

[40] T. Xie, F. Bourdatot, T. Fennell, H. Luo, L.-P Regnault, and T. Weber (2018), Institut Laue-Langevin (ILL), doi:10.5291/ILL-DATA.4-02-532.